Chemical and Biological Impacts of Ocean Acidification Along the West Coast of North America

Richard A. Feely[a*], Simone Alin[a], Brendan Carter[b], Nina Bednaršek[c], Burke Hales[d], Francis Chan[e], Tessa M. Hill[f,g], Brian Gaylord[f], Eric Sanford[f], Robert H. Byrne[h], Christopher L. Sabine[a], Dana Greeley[a], and Lauren Juranek[d]

[a]NOAA Pacific Marine Environmental Laboratory, 7600 Sand Point Way NE, Seattle, WA 98115, USA

[b]Joint Institute for the Study of the Atmosphere and Ocean, University of Washington, Seattle, WA 98195, USA

[c]School of Marine and Environmental Affairs, University of Washington, Seattle, WA 98195, USA (previously at NOAA Pacific Marine Environmental Laboratory)

[d]College of Oceanic and Atmospheric Sciences, Oregon State University, Corvallis, OR 97331, USA

[e]Department of Integrative Biology, Oregon State University, Corvallis, OR 97331, USA

[f] Bodega Marine Laboratory, University of California Davis, Bodega Bay, CA 94923, USA.

[g]Department of Earth and Planetary Sciences, University of California Davis, Davis, CA 95616, USA

[h]College of Marine Science, University of South Florida, 140 7th Avenue South, St. Petersburg, FL 33701, USA

- Corresponding author: Richard.A.Feely@noaa.gov

Keywords: California Current Large Marine Ecosystem, Ocean Acidification, Anthropogenic CO_2, Upwelling, Pteropod Dissolution

Abstract

The continental shelf region off the west coast of North America is seasonally exposed to water with a low aragonite saturation state by coastal upwelling of CO_2-rich waters. To date, the spatial and temporal distribution of anthropogenic CO_2 (C_{anth}) within the CO_2-rich waters is largely unknown. Here we adapt the multiple linear regression approach to utilize the GO-SHIP Repeat Hydrography data from the northeast Pacific to establish an annually updated relationship between C_{anth} and potential density. This relationship was then used with the NOAA Ocean Acidification Program West Coast Ocean Acidification (WCOA) cruise data sets from 2007, 2011, 2012, and 2013 to determine the spatial variations of C_{anth} in the upwelled water. Our results show large spatial differences in C_{anth} in surface waters along the coast, with the lowest values (37–55 μmol kg^{-1}) in strong upwelling regions off southern Oregon and northern California and higher values (51–63 μmol kg^{-1}) to the north and south of this region. Coastal dissolved inorganic carbon concentrations are also elevated due to a natural remineralized component (C_{bio}), which represents carbon accumulated through net respiration in the seawater that has not yet degassed to the atmosphere. Average surface C_{anth} is almost twice the surface remineralized component. In contrast, C_{anth} is only about one third and one fifth of the remineralized component at 50 m and 100 m depth, respectively. Uptake of C_{anth} has caused the aragonite saturation horizon to shoal by approximately 30–50 m since the preindustrial period so that undersaturated waters are well within the regions of the continental shelf that affect the shell dissolution of living pteropods. Our data show that

47 the most severe biological impacts occur in the nearshore waters, where corrosive waters
48 are closest to the surface. Since the pre-industrial times, pteropod shell dissolution has, on
49 average, increased approximately 20–25% in both nearshore and offshore waters.
50
51 **1. Introduction**
52 Since the beginning of the Industrial Revolution, the global oceans have absorbed about
53 28% (~550 billion tons) of the total anthropogenic carbon dioxide (CO_2) emissions
54 (Canadell et al., 2007; IPCC, 2013). This absorption of atmospheric CO_2 has increased
55 ocean acidity in a process referred to as "anthropogenic" ocean acidification (OA). Over
56 the past 250 years, the pH of open-ocean surface waters has decreased by approximately
57 0.11 units, equivalent to an increase of about 28% in hydrogen ion concentration (Gattuso
58 et al., 2015). When CO_2 enters the ocean, it reacts with water to form carbonic acid,
59 which consumes carbonate ions (CO_3^{2-}) via the release of protons. In direct
60 correspondence with these changes, the CO_3^{2-} concentration has declined about 16%
61 from preindustrial values through the year 2000. By the end of this century, surface ocean
62 pH is expected to decline by another 0.3–0.4 units, and CO_3^{2-} concentration is expected to
63 decline by ~50% (Feely et al., 2004, 2009; Orr et al., 2005; Doney et al., 2009a,b;
64 Gattuso et al., 2015).
65
66 Organisms that produce calcium carbonate ($CaCO_3$) shells or skeletons made of aragonite
67 or calcite are expected to encounter increasing physiological challenges as the saturation
68 state of aragonite and calcite decreases due to OA (Fabry et al., 2008; Guinotte and
69 Fabry, 2008; Hofmann and Todgham, 2010; Gaylord et al., 2011; Barton et al., 2012;

Bednaršek et al., 2012a, 2014a,b; Hettinger et al., 2012; Frieder et al., 2014; Gattuso et al., 2015; Waldbusser et al., 2015; Somero et al., 2016). The saturation state of aragonite (Ω_{ar}) and calcite (Ω_{cal}) is a function of the concentrations of calcium (Ca^{2+}) and CO_3^{2-}, and pressure-dependent stoichiometric solubility product, K_{sp}^*: ($\Omega = [Ca^{2+}][CO_3^{2-}]/ K_{sp}^*$) (Mucci, 1983), such that Ω_{ar} and Ω_{cal} will decline as more CO_2 is taken up by the oceans. At Ω=1, carbonate minerals are in equilibrium with surrounding seawater; at Ω>1, precipitation or preservation of carbonate minerals is thermodynamically favored; and at Ω<1, dissolution is favored.

Recent models suggest that the shallower waters along the California Current Large Marine System (CCLME) will become undersaturated more often and for longer durations over the next several decades to a century (Gruber et al. 2012; Hauri et al., 2013; Turi et al., 2016). Persistence of acidified water in the coastal waters of the west coast of North America could have profound consequences for marine organisms, ecosystems, and the ecosystem services of this region (Doney et al., 2009a; Gattuso and Hansson, 2011; Feely et al., 2012a; Ekstrom et al., 2015; Gaylord et al., 2015; Somero et al., 2016). Increasing CO_2 may have significant biological and ecological effects, with potential feedbacks to biogeochemical cycles. Declines in $CaCO_3$ saturation state, particularly Ω_{ar}, will pose increasing physiological challenges to calcifying invertebrates such as pteropods, bivalves, and echinoderms (Wooton et al., 2008; Hettinger et al., 2012; Kroeker et al., 2013; Frieder et al., 2014; Bednaršek et al., 2012a; 2014a,b; Waldbusser et al., 2015; Barton et al., 2015; Somero et al., 2016).

Pteropods are an important food source for organisms across lower (e.g.macrozooplankton) and higher trophic levels in the oceans. In the North Pacific Ocean, pteropods are seasonally substantial portion of the diets of pink and chum salmon (Groot and Margolis, 1991), sablefish and rock sole (Armstrong et al., 2005; Aydin et al., 2005). Moreover, they are among the species most affected by ocean acidification, with shell dissolution already occurring in the natural environment (Bednaršek et al., 2014a). Consequently, pteropods are ideal sentinel organisms to study how the changes since the pre-industrial times are affecting aragonite dissolution in the CCLME, and help to identify which of the regions are the most vulnerable to the anthropogenic changes. In this paper we estimate the amount of anthropogenic CO_2 (C_{anth}) in the CCLME region and determine its impact on pteropod shell dissolution comparatively for cruises in 2011 and 2013.

1.1. Physical and biogeochemical setting

The CCLME is a large-scale oceanographic feature along the west coast of North America, an eastern boundary current extending from northern Vancouver Island in Canada to Punta Eugenia in Mexico, and landward into large estuarine systems such as the San Francisco Bay and the Salish Sea (Fig. 1). The coastal waters off the west coast of North America are strongly affected by seasonal upwelling, which typically begins in early spring when the Pacific High moves into the subarctic North Pacific, resulting in a strengthening of the northwesterly winds. These winds drive net surface waters offshore via Ekman transport, which induces the upwelling of low pH, nutrient- and CO_2-rich, intermediate depth (100 to 300 m) offshore waters onto the continental shelf (Hales et al.,

2006; Feely et al., 2008; Gruber et al., 2012; Harris et al., 2013; Hauri et al., 2013; Turi et al., 2016). The upwelling lasts from spring to early or late fall, when winter storms return. Within the CCLME, the upwelling supports highly productive communities and fisheries on the continental shelf and slope, and in the estuaries (Hickey, 1979; Thomson et al., 1989; Thomson and Krassovski, 2010). Thus, while upwelling plays a defining role in CCLME biogeochemistry, productivity, and ecology, it also contributes to the impacts of local and regional oceanographic processes that exacerbate the effects of anthropogenic OA. Here we use the term "corrosive" to refer to waters that are undersaturated with respect to aragonite ($\Omega_{ar}<1$), a condition that results from some combination of: 1) oceanic uptake of anthropogenic CO_2, and 2) build-up of CO_2 from the natural respiration processes in the ocean interior (C_{bio}) that occur in offshore waters prior to upwelling or on the continental shelf after those interior waters have upwelled. These processes are already affecting coastal regions such that corrosive waters have previously been observed in large coastal regions including Arctic and Alaskan coastal waters, as well as the CCLME (Feely et al., 2008; Bates et al., 2013; Mathis et al., 2014a,b, 2015).

Many of the ecosystems within the CCLME are particularly vulnerable because of the combined effects of acidification, warming, upwelling, and hypoxia, which are expected to increase under anthropogenic climate change (Rykaczewski and Dunne, 2010; Somero et al., 2016). The term "hypoxia" implies diminished levels of oxygenation under which many species of fish and invertebrates are negatively impacted. Conditions ranging from hypoxic (<65 μmol kg^{-1}) to anoxic (0 μmol kg^{-1}) have been observed in near-bottom waters on the inner continental shelf within the CCLME, particularly in the late summer

and early fall months when respiration-induced oxygen depletions are at their maximum extent (Grantham et al., 2004; Hales et al., 2006; Chan et al., 2008; Booth et al., 2012; Siedlecki et al., 2016). High CO_2 concentrations and hypoxia are linked mechanistically because aerobic respiration of organic matter consumes oxygen and produces CO_2 in approximate stoichiometric equivalence (170:117) (Anderson and Sarmiento, 1994). Thus, processes that create aquatic oxygen deficits can also exacerbate corrosive conditions for calcareous organisms.

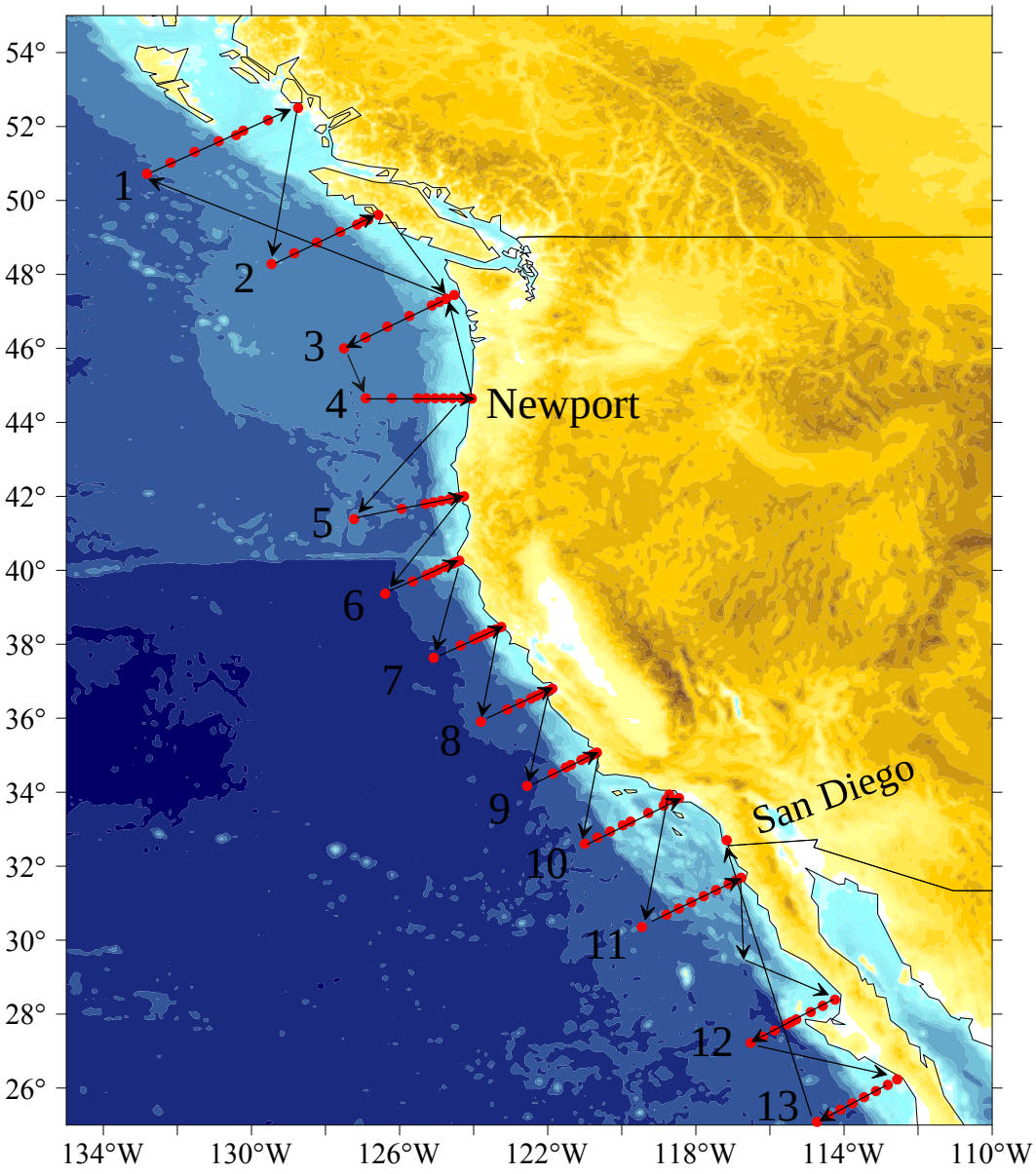

145

146 Figure 1. Map of the station locations for the 2007 West Coast cruise. The black line

147 shows the cruise track. The 2011, 2012, and 2013 cruises included subsets of these

148 stations and, in some cases, a few additional stations.

2. Analytical methods

2.1. Chemical methods

In the late spring of 2007 and late summers of 2011, 2012, and 2013 we conducted detailed observations of carbonate system chemistry and other physical, chemical, and biological parameters along the western North American continental shelf, both via ship-based cruises and shore-based sampling (Fig.1). Water samples from the cruises were collected in modified Niskin-type bottles and analyzed under laboratory conditions for dissolved inorganic carbon (DIC), total alkalinity (TA), oxygen, and nutrients. During the cruises in 2011 and 2013, samples were also measured directly for pH_T. DIC was analyzed using coulometric titration (Johnson et al., 1987; DOE, 1994; Ono et al., 1998). TA was measured by the potentiometric titration method (Millero et al., 1993; DOE, 1994; Ono et al., 1998). Certified Reference Materials were analyzed with both the DIC and TA samples as an independent verification of instrument calibrations (Dickson et al., 2007). The ship-based DIC and TA data are both precise and accurate to within 2 µmol kg^{-1}. The spectrophotometric method described in Byrne et al. (2010) and Liu et al. (2011) was used to measure pH on the total scale (pH_T) for the 2011 and 2013 cruises. Shore-based measurements of pH_T from *in-situ* sensors and DIC and TA from discrete samples were also provided through the OMEGAS (8 sites) and UC Davis Coastal Transect (47 sites) projects, respectively. *In-situ* records were collected using Durafet®-based sensors that were calibrated against seawater and/or TRIS-based Certified Reference Materials. Bottle samples were analyzed for DIC (via infrared CO_2; Monterey Bay Aquarium Research Institute) and TA (Metrohm 855 autotitrator), and were cross-

verified with pH determined spectrophotometrically for pH, using the total pH scale. The saturation state of seawater with respect to aragonite was calculated from the DIC and TA data using the program CO2SYS developed by Lewis and Wallace (1998), using the Lueker et al. (2000) carbonate constants, Dickson (1990) for the KSO4, and Lee et al. (2010) for total boron. The pressure effect on the solubility, for samples collected at depth, is estimated from the equation of Mucci (1983), incorporating adjustments to the constants recommended by Millero (1995). Based on the uncertainties in the DIC and TA measurements and the thermodynamic constants, the uncertainty in the calculated Ω_{ar} is approximately 0.02. Oxygen analysis was conducted by modified Winkler titration (Carpenter, 1965), and nutrients (nitrate, nitrite, ammonium, phosphate, silicate) were frozen at sea and analyzed using a Technicon AutoAnalyzer II (UNESCO, 1994) at Oregon State University.

2.2. Pteropod shell dissolution

Pteropod shell dissolution was determined on shells collected from 16 stations for the 2011 cruise and 20 stations during the 2013 cruise. The samples were stored in 90% buffered ethanol. Between 15 to 30 pteropods of *Limacina helicina* were blindly picked from samples selected randomly with no prior knowledge of station location or carbonate chemistry conditions. Following the methods described in Bednaršek et al. (2012c), the shells were repeatedly washed with distilled water before being subjected to chemical shell dehydration, followed by a plasma etching procedure for periostracum removal. All treated shells were analyzed for shell dissolution using a scanning electron microscope (SEM) and identified for the presence of dissolution patterns and the proportion of more

195 severe types of shell dissolution (Type II and Type III). Following the categorization
196 scheme outlined in Bednaršek et al. (2012c), Type II dissolution indicates deeper
197 penetrating dissolution that precedes Type III, which affects large parts of shell
198 crystalline structure, making shells less compact and more fragile.
199
200 **2.3. Estimating coastal C_{anth} and C_{bio}**
201 Seawater upwelling along the continental shelf of the west coast of North America comes
202 from the thermocline waters of the North Pacific subtropical and subarctic gyres. We
203 therefore used the gyre thermocline C_{anth}, estimated by Carter et al. (submitted)
204 employing the methods outlined in Supplementary Materials section SM1.1 (this paper) -
205 to estimate upwelling water C_{anth} for the years 2007, 2011, 2012, and 2013. This method
206 is similar to the approach for used by Feely et al. (2008). Our approach for estimating
207 coastal C_{anth} and biological remineralization C (C_{bio}) involves the following steps:
208 1. Open ocean C_{anth} estimates are used to derive polynomials relating thermocline C_{anth}
209 to potential density σ_θ for both 2004 and 2013 along P02 (two polynomials) and in
210 2006 and 2015 along P16N (two additional polynomials). See Supplementary
211 Materials section SM1.2 for details on this step.
212 2. A grid of seawater properties shoreward of the 200 m depth isobath is determined
213 along the West Coast from our hydrographic surveys in 2007, 2011, 2012, and 2013
214 using the procedure detailed in the Supplementary Materials section SM1.3.
215 3. The four polynomials determined in step 1 are used with the σ_θ estimates determined
216 in step 2 to estimate C_{anth} for all gridded locations.

4. We interpolate among the four estimates from step 3 to obtain sets of estimates specific to the 4 years of interest (2007, 2011, 2012, and 2013) at each location. We interpolate among the four polynomials both by date to select between the earlier and later polynomials for each section, and by gridded seawater spiciness to select between the P02 and P16 polynomials.
5. We directly estimate C_{bio}, or the amount of additional DIC present as a result of organic matter remineralization, from seawater properties using methods described in detail in Supplementary Materials SM1.2.

These gridded properties are used for volume-weighted seawater average properties. Also in SM1.2, the uncertainties in these quantities are estimated to be of order ± (1σ) 10 μmol kg^{-1}, yielding a 95% confidence interval of ~20 μmol kg^{-1}. We refer to the sum of C_{anth} and C_{bio} as "enriched DIC."

3. Results

3.1. Coastal distributions of acidified water

During the four cruises, various stages and strengths of upwelling were observed from central Vancouver Island, Canada to Baja California, Mexico. The observations revealed that, on average, acidified, corrosive CO_2-rich waters (*insitu* pH_T < 7.75; Ω_{ar} <1.0; DIC > 2190 μmol kg^{-1}) were upwelled from depths of 150–250 m to depths as shallow as 20–200 m in most areas and close to the surface in the region between northern California near Cape Mendocino to Heceta Head, Oregon (Figs. 2–4). Maps of surface ocean pH_T and DIC during the four West Coast survey cruises show that *insitu* pH_T values ranged from 7.7 to 8.3, with the lowest pH_T values and highest DIC concentrations occurring in

240 the upwelled water near the coast (Figs. 2 and 3). Moving offshore, pH_T values quickly
241 increase to open-ocean values ranging from 8.0 to 8.3. The 2011 pH_T map includes
242 complementary shore-based nearshore and intertidal pH_T data from the same period,
243 collected using Durafet-style autonomous sensors (Fig. 2), which reinforces the notion
244 that the greatest spatial variability of pH_T appears in closest proximity to the shore (Chan
245 et al., submitted). The excellent consistency among the intertidal, nearshore, and offshore
246 data suggests that the uptake of anthropogenic CO_2, upwelling/mixing, and respiration
247 processes are the primary drivers of pH_T distributions along the coast. Our results for the
248 four cruises follow the seasonal patterns described by Chan et al. (submitted) from field
249 data. Consistent with those results, Turi et al (2016) found similar patterns in their
250 hindcast biogeochemical model outputs, with higher pH values in the spring and lower
251 pH values in the late summer. One exception is the low pH_T, high O_2, low Ω_{ar} values in
252 surface waters immediately seaward of the Columbia River Estuary in 2011, 2012, and
253 2013, which were dominated by the outflow of low salinity, low alkalinity, and high DIC
254 riverine water in the surface layer (Evans et al., 2013).

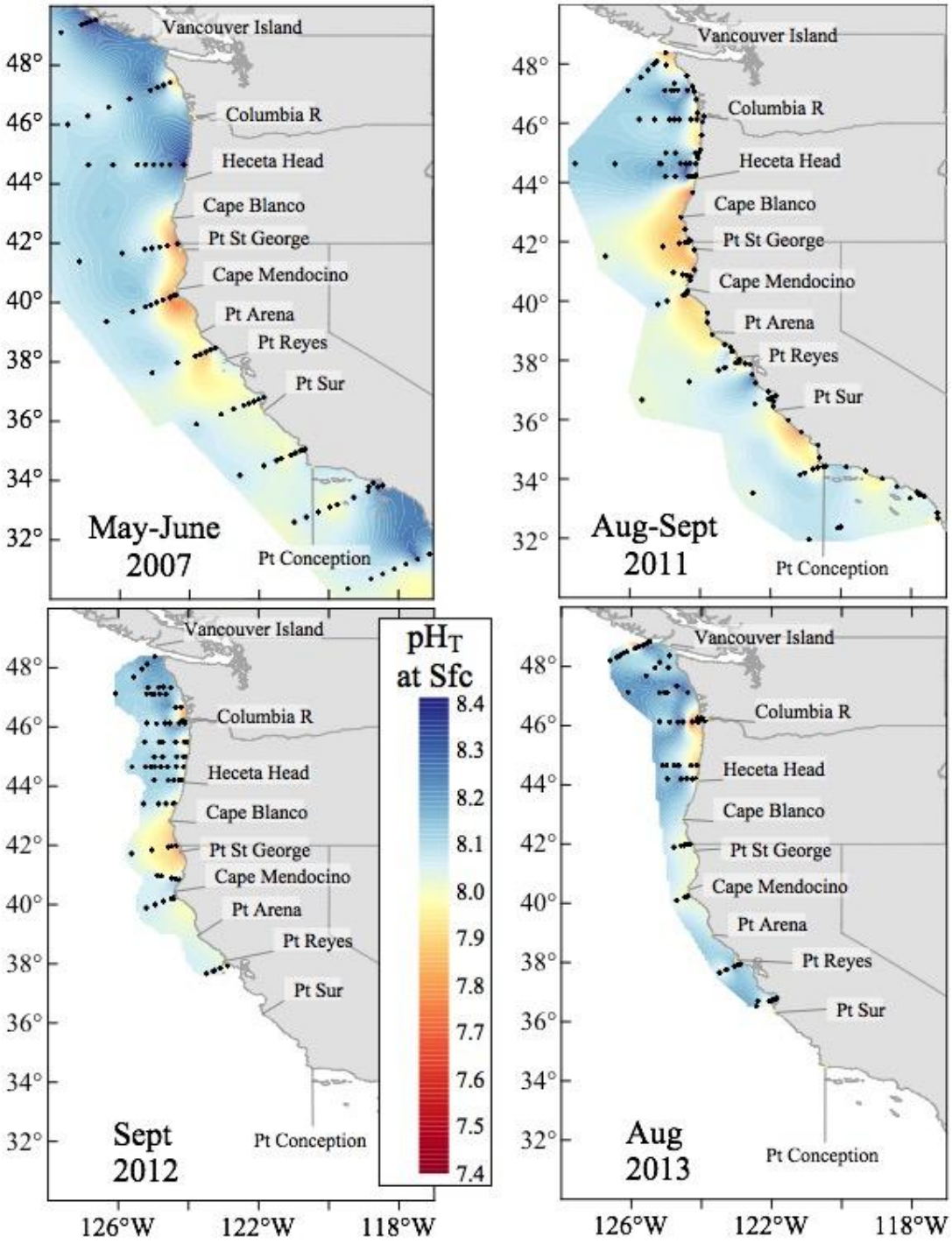

255

256 Figure 2. Maps of surface ocean pH_T values for the 2007, 2011, 2012, and 2013 cruises.

257 The 2011 map includes the shore-based intertidal data.

258

259 The corrosive waters along the inner- and mid-shelf regions were due to the combined
260 impacts of anthropogenic CO_2 uptake and upwelling of respiration-enriched CO_2 waters
261 along the coast (Figs. 4 and 5). Nearshore upwelled waters were characterized by low-pH
262 seawater (pH <7.75) with Ω_{ar} values near or below 1.0 and potential density >26.0 kg m^3.
263 In 2013, for example, along Line 6 offshore of Newport, Oregon, the 26.1 kg m^3 potential
264 density surface shoaled from a depth range of 150–200 m offshore to the surface near the
265 coast (Fig. 5). This density surface was co-located with isolines of Ω_{ar} = 1.0, DIC = 2190
266 µmol kg^{-1}, and pH = 7.75. However, pH decreased, and DIC and the partial pressure of
267 CO_2 (pCO_2) increased shoreward in the region surrounding this isopycnal due to CO_2
268 release from local remineralization of organic matter. Upwelling of CO_2-enriched
269 seawater caused the entire water column shoreward of the 50 m isobath along Line 6 to
270 become undersaturated with respect to aragonite (Fig 5D). The lowest Ω_{ar} values (<0.70)
271 found shoreward of the 200 m isobath were observed in the near-bottom waters of the
272 mid-shelf region where respiration provides an additional CO_2 contribution that decreases
273 Ω_{ar}. The uptake of anthropogenic CO_2 has caused the corrosive (Ω_{ar} <1) waters to shoal
274 by about 30–50 m since preindustrial times such that they are within the density layers
275 that are currently being upwelled along the west coast of North America (Feely et al.,
276 2012b).
277

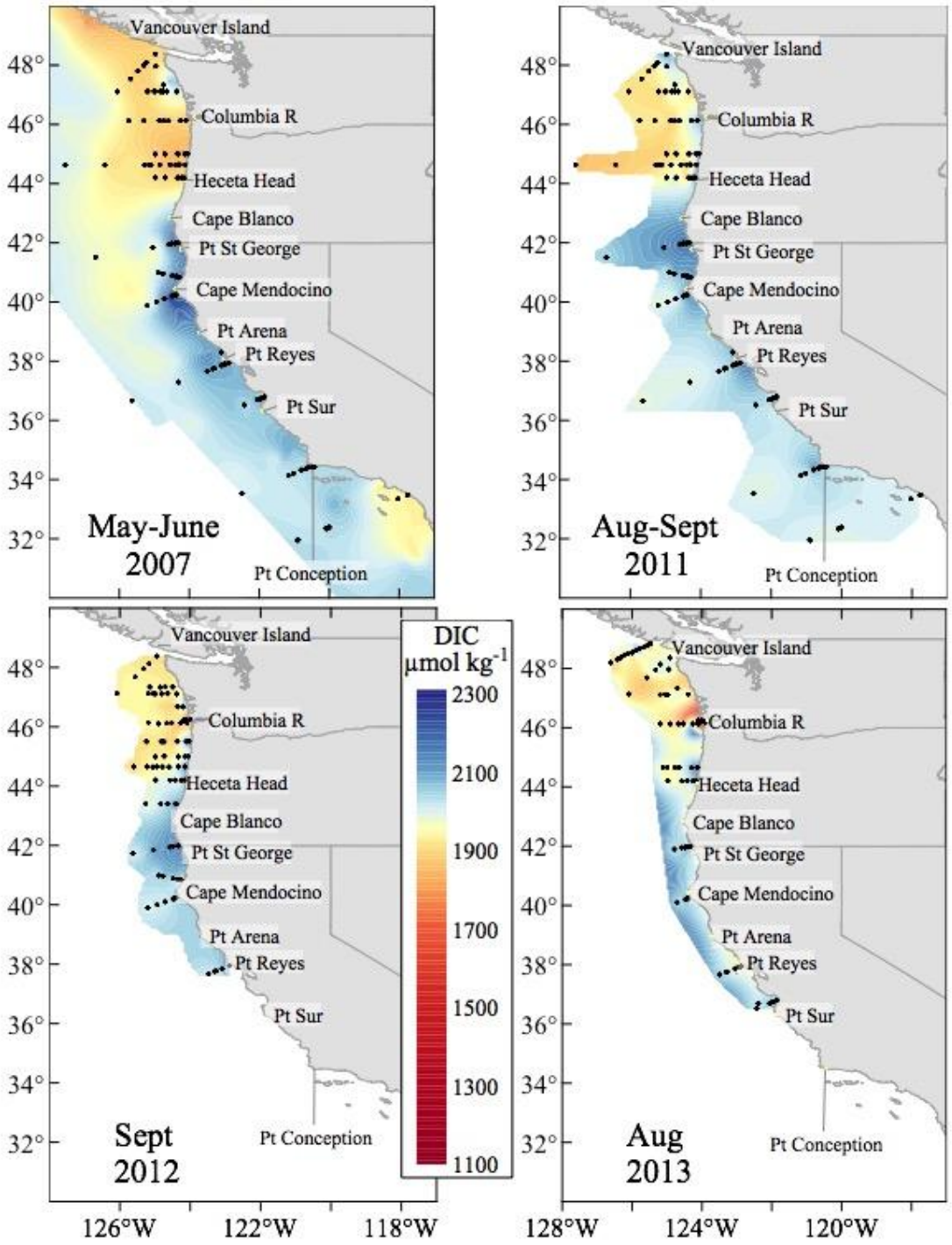

278

279 Figure 3. Maps of surface DIC concentrations in µmol kg^{-1} for the 2007, 2011, 2012, and

280 2013 cruises. The nearshore upwelling regions are delineated by DIC concentrations in

281 excess of 2050 µmol kg^{-1}. Black dots indicate measurement locations. Open circles on the

282 2011 and 2013 cruises indicate stations where both chemical and biological samples were

283 taken.

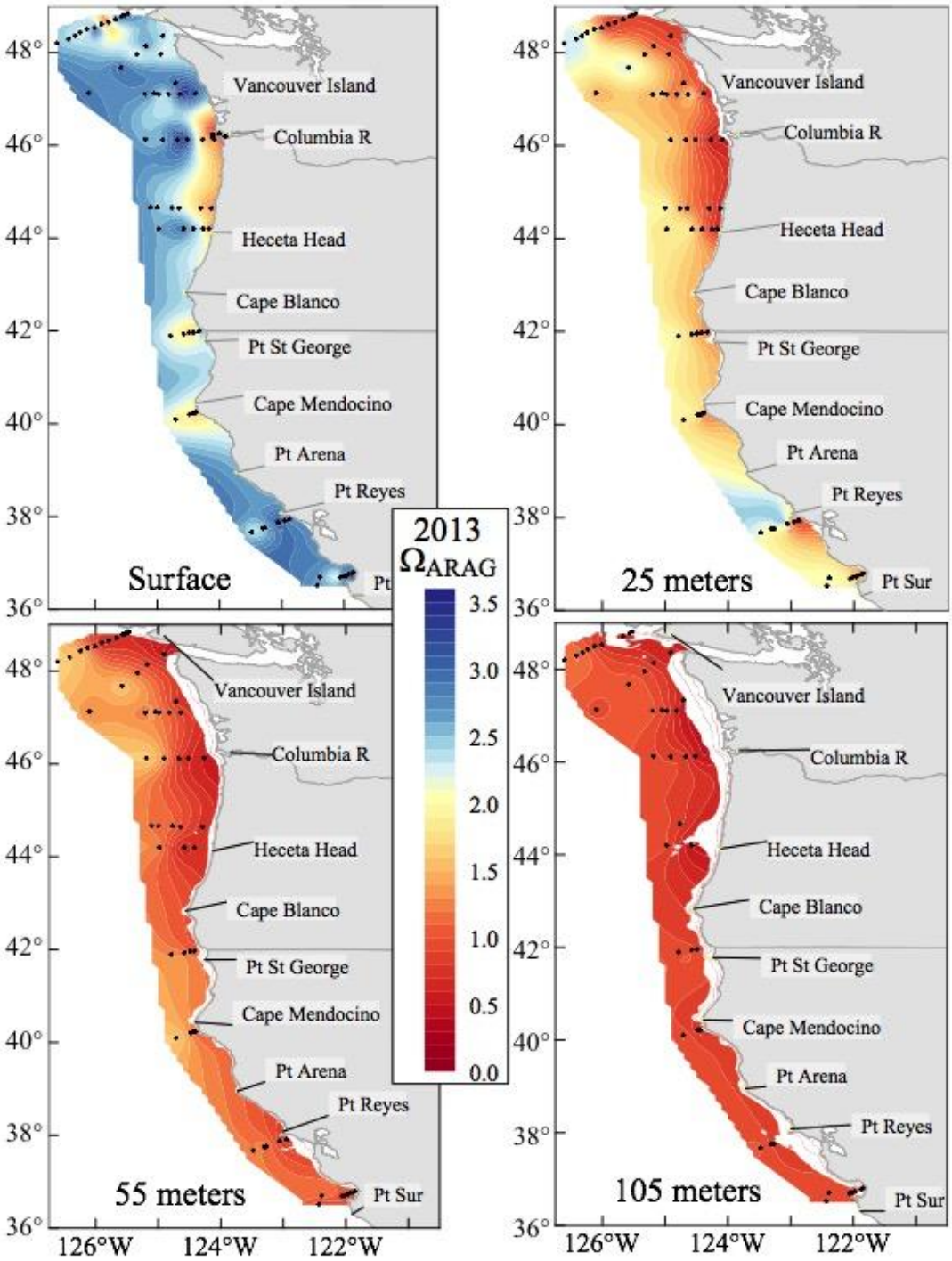

284

285 Figure 4. Aragonite saturation state at the surface, 25 m, 55 m, and 105 m depth during

the 2013 West Coast survey.

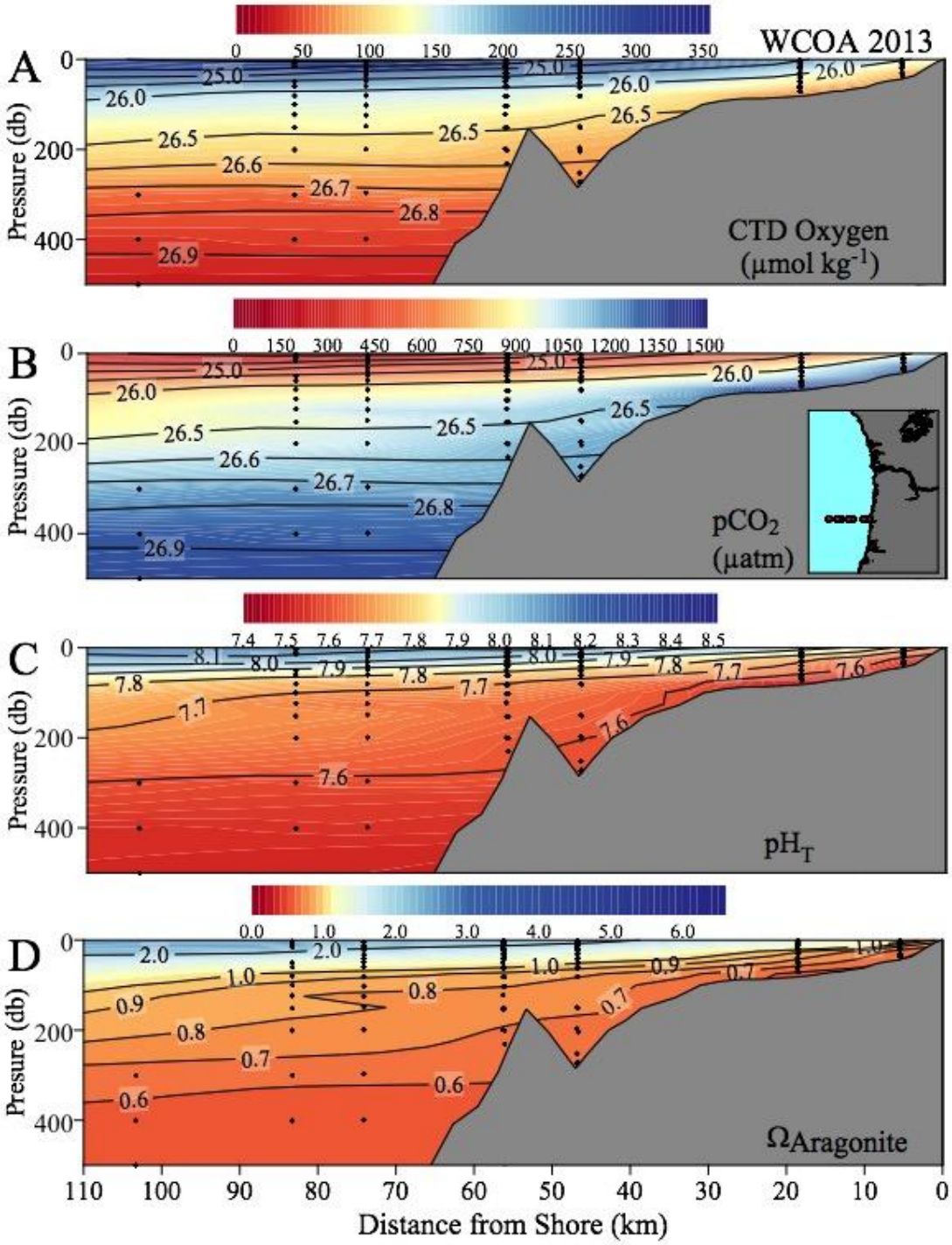

Figure 5. Vertical sections of: (A) dissolved oxygen, (B) pCO_2, (C) pH_T, and (D) Ω_{ar}

290 along the 2013 Line 6 stations off Newport, OR. Black dots indicate measurement
291 locations and the isolines lines in (A) and (B) show the potential density in kg m^{-3}.
292
293 **3.2. Pteropod dissolution and water chemistry**
294 The water column hydrographic data were combined with the chemical data for the
295 nearshore and offshore regions and the aragonite saturation state (Ω_{ar}) was calculated for
296 the upper 55 m or 100 m of the water column in the nearshore and offshore, respectively.
297 Diel vertical migration of *L. helicina* is within this depth range. The values from the
298 region off Southern California were not taken into account, as we did not have pteropod
299 dissolution data for that region. There was a strong negative linear correlation between
300 the percentage of pteropods with Type II and Type III dissolution shell impacts and Ω_{ar} in
301 2011 and 2013 (Fig. 6, R^2=0.74, $p< 0.001$). We have fitted the combined data (2011 and
302 2013) to a logarithmic function and generated the equation: $y = -66.29 \ln x + 61.21$ (R^2 =
303 0.74). This relationship was used for estimating the percentage of individuals with severe
304 dissolution for both pre-industrial and current Ω_{ar} values (Table 2).

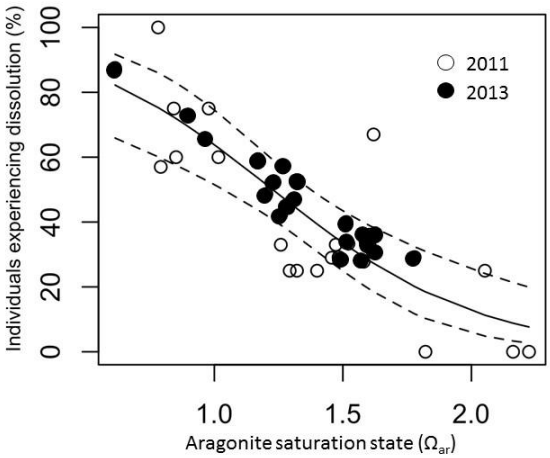

Figure 6. Percentage of individuals affected by severe dissolution as a function of aragonite saturation state (integrated over the upper100 m) for the 2011 (open circles) and 2013 (closed circles) data. The dashed lines show the 95% confidence interval for the logarithmic function.

During both 2011 and 2013 cruises, pteropod shell dissolution was observed to be significantly higher in the nearshore region of the CCLME. Currently, on average 57% of individuals are affected by dissolution in the nearshore regions, but only 36% in the offshore region (Table 2). This greater incidence of dissolution-affected individuals is consistent with lower aragonite saturation state in the nearshore region (average Ω_{ar} = 1.07) compared to the offshore region (average Ω_{ar} = 1.47).

4. Discussion

4.1. Estimates of C_{anth} and C_{bio} in the CCLME

320 Because the increased DIC concentrations along the coast are the result of uptake of C_{anth}
321 and upwelling of CO_2-rich respired CO_2 (C_{bio}) waters from below we have estimated the
322 contributions of both C_{anth} and C_{bio} throughout the water column. Our estimates of the
323 distribution of C_{anth} from the coast out to the open-ocean for 2013 are presented as maps
324 for surface, 25, 55, and 105 m (Fig. 7), and a summary of the regional averages are given
325 in Table 1. In nearshore surface waters, C_{anth} ranges from about 37 to 60 µmol kg^{-1}, with
326 increasing concentrations north and south of the region near Cape Blanco. The lowest
327 C_{anth} concentrations (ranging from 37 to 55 µmol kg^{-1}) are centered near the strong
328 upwelling center between the region south of the Columbia River to Cape Mendocino. To
329 the north and south of this region nearshore C_{anth} concentrations are somewhat higher,
330 indicating mixing of the upwelled water with water that has been in recent contact with
331 the atmosphere. The highest C_{anth} concentrations (ranging from 44 to 63 µmol kg^{-1}) are
332 located in the offshore surface waters. At 25 m in the nearshore region, the influence of
333 the upwelled water is more pronounced, with C_{anth} concentrations ranging from 33 to 55
334 µmol kg^{-1} along most of the coastline. At deeper nearshore depths, C_{anth} ranges from 33
335 to 56 µmol kg^{-1} at 55 m and from 29 to 53 µmol kg^{-1} at 105 m.
336
337 Average C_{anth} and C_{bio} concentrations are shown in Figure 8 and a summary of the
338 regional and depth averages for C_{anth} and C_{bio} is given in Table 1. For comparison, Table
339 1 also shows enriched carbon contributions found at the surface and at 200 m depth at the
340 most northwestern station (i.e., most offshore) within each study region. In offshore
341 surface waters, nearly all of the enriched DIC ($C_{anth} + C_{bio}$) is from C_{anth}, whereas at 200 m
342 only about 19% of the enriched DIC is from C_{anth} and the remainder is from C_{bio}.

In the nearshore region of the CCLME, enriched DIC in surface waters ranged from 41 to 148 μmol kg^{-1}, with an average of about 65% of enriched DIC in the surface waters due to C_{anth} and the remainder due to C_{bio}. Enriched DIC at 50 m is larger than at the surface (range: 129 - 172 μmol kg^{-1}), but the percentage due to C_{anth} is lower (~32%). Finally, at 100 m, only about 22% of the enriched DIC is due to C_{anth}. There is some year-to-year variability within the regions but the highest contributions of C_{anth} and total enriched-DIC generally occur in the later years. While the percentage of C_{anth} in the nearshore upwelled water is lower than the surrounding water, the total amount of enriched DIC is highest in the nearshore upwelled water and, consequently, those nearshore upwelled waters are the most corrosive to calcifying organisms. In subsurface waters, the most corrosive conditions occur in the onshore bottom waters within 20 km of the coast. The uptake of C_{anth} has caused the aragonite saturation horizon to shoal by approximately 30–50 m since the preindustrial period so that undersaturated waters are well within the regions of the continental shelf that affect the shell dissolution of living pteropods (Feely et al., 2008).

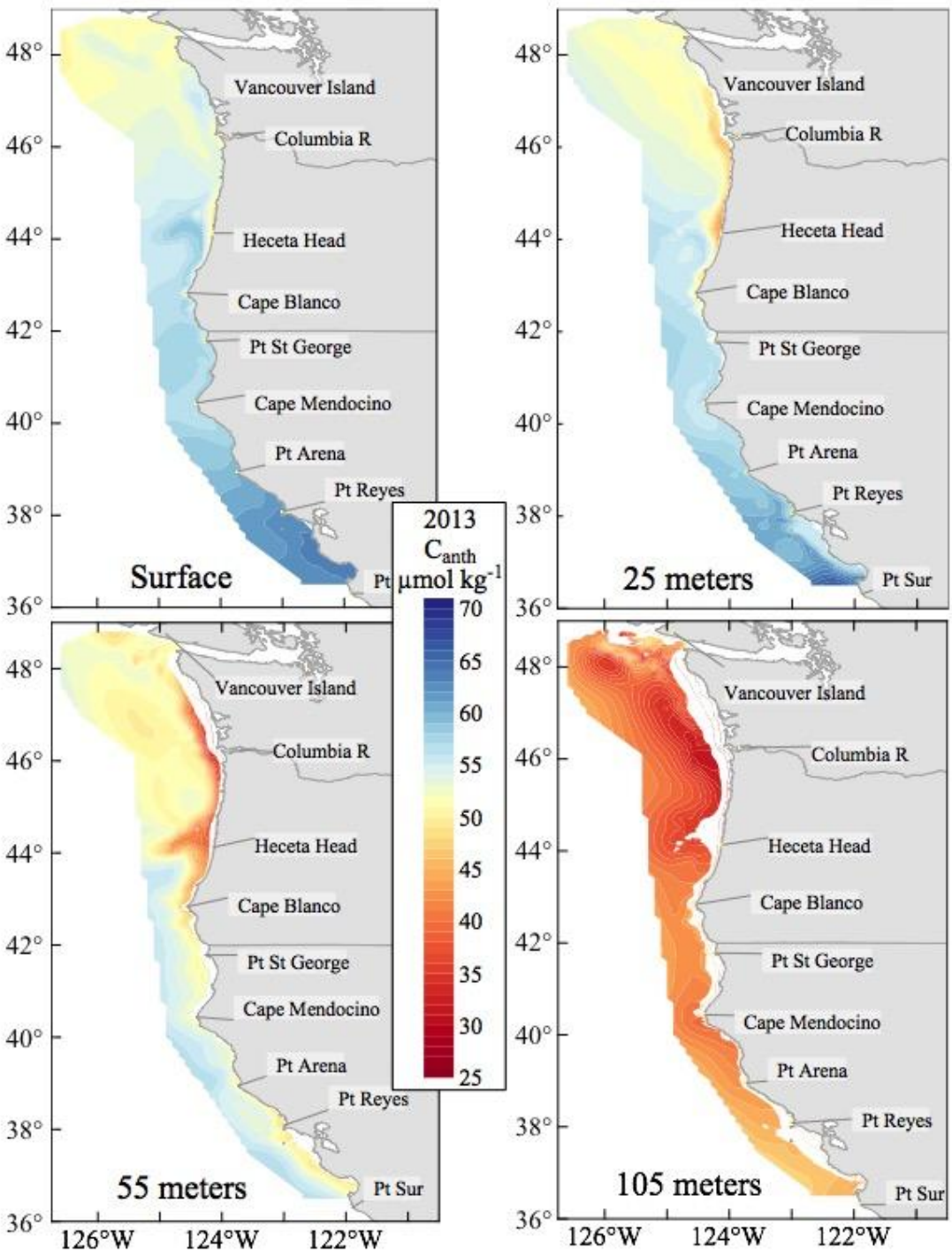

360

361 Figure 7. Distribution of C_{anth} in µmol kg^{-1} at the surface, 25 m, 55 m, and 105 m depth

362 for the 2013 West Coast survey.

Table 1. Anthropogenic carbon (C_{anth}), remineralized carbon (C_{bio}) and anthropogenic percentage of total enriched carbon ($\%C_{anth}$) by region (W: Washington, O: Oregon, NC: Northern California, SC: Southern California), cruise year, and depth for averages of gridded coastal properties shoreward of the 200 m isobath (left columns) and for the northwestern stations occupied offshore of each region (right columns). All values are expressed in μmol kg^{-1}. Estimated average uncertainty is approximately ±10 μmol kg^{-1} (1σ). Column averages are calculated weighting all regions and years equally. Negative C_{bio} values suggest either net autotrophy or physically derived oxygen supersaturation.

		Grid average shoreward of 200 m isobath									*Northwestern station in region*					
Depths		0-10 m			50-60 m			100-110 m			Surface			200 m		
State	Year	C_{anth}	C_{bio}	$\%C_{anth}$	C_{anth}	C_{bio}	$\%C_{anth}$	C_{anth}	C_{bio}	$\%C_{anth}$	C_{anth}	C_{bio}	$\%C_{anth}$	C_{anth}	C_{bio}	$\%C_{anth}$
W	2007	47	-27	232	47	85	35	34	131	21	47	-5	113	30	140	18
W	2011	51	97	34	47	125	27	36	149	20	54	0	101	33	133	20
W	2012	52	83	39	49	117	29	36	150	19	55	-7	114	30	154	16
W	2013	53	48	53	48	111	30	39	153	20	55	-6	113	31	159	16
O	2007	47	24	66	44	93	32	34	147	19	48	-9	122	32	117	21
O	2011	52	31	62	42	114	27	34	158	18	52	-5	112	35	99	26
O	2012	54	18	75	48	88	35	39	131	23	53	-1	102	33	143	19
O	2013	55	37	60	46	121	27	37	149	20	56	-7	115	33	141	19
NC	2007	37	32	54	33	96	26	29	135	18	44	-10	128	27	134	17
NC	2011	57	49	54	47	108	30	42	138	23	56	-5	110	27	157	15
NC	2012	58	28	68	53	82	39	49	112	30	56	4	94	33	140	19
NC	2013	60	17	78	52	97	35	43	137	24	58	-8	115	33	139	19
SC	2007	55	-22	167	43	116	27	38	135	22	51	-6	114	32	153	17
SC	2011	59	28	68	56	56	50	53	82	39	58	0	99	42	95	31
SC	2012	-	-	-	-	-	-	-	-	-	60	-9	117	37	155	19
SC	2013	-	-	-	-	-	-	-	-	-	63	-31	196	37	157	19
Averages		53	28	65	47	102	32	39	136	22	54	-7	115	33	139	19

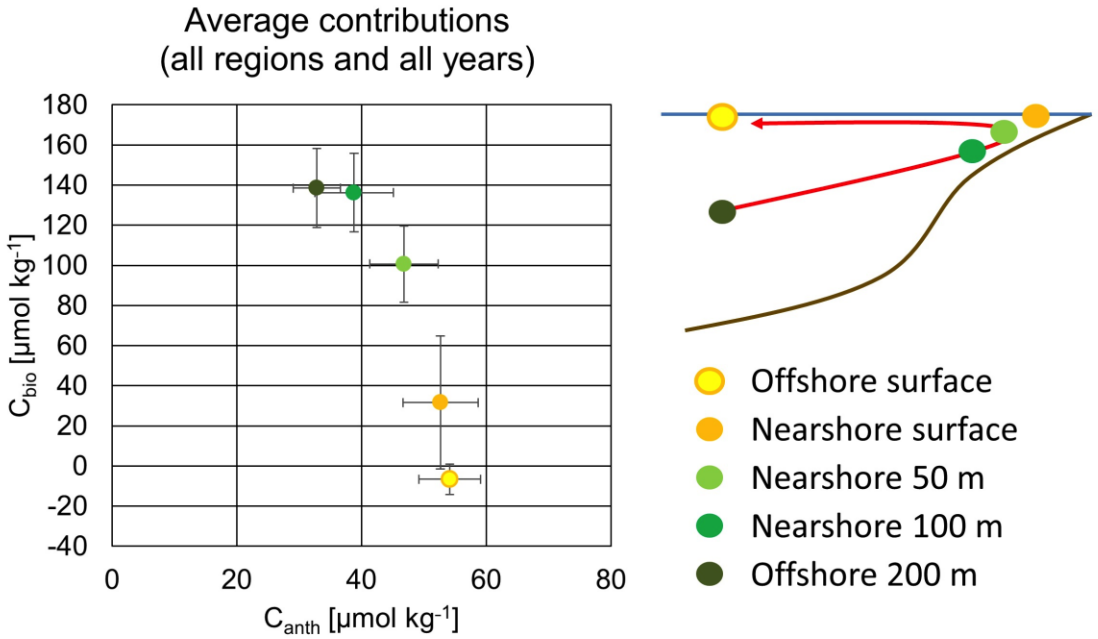

363

364 Figure 8. Plot of C_{bio} vs C_{anth} in offshore and nearshore waters in the California Current
365 Large Marine Ecosystem. The simple schematic in the upper right is a cross section of the
366 coast with offshore being to the left, and with the mean path of upwelling water indicated
367 as a red arrow. Error bars express standard deviations for various estimates from each
368 region and depth (Table 1) rather than uncertainty, which is approximately ±10 µmol
369 kg^{-1} (1σ) for C_{bio} and C_{anth}.

370

371 **4.2. Biological impacts evaluated as pteropod shell dissolution**

372 Co-locating biological responses and chemical observations allows for direct
373 comparison of results in 2011 and 2013. Pteropod dissolution has been found to be
374 highly correlated with aragonite saturation conditions in 2011 (Bednaršek et al., 2014a).
375 Consequently, we have used the same procedure to also correlate the extent of dissolution
376 also for 2013. Pteropod shell dissolution significantly increased from offshore to
377 nearshore in the CCLME. Pteropods were ~22% more likely to be affected by severe

shell dissolution in nearshore waters compared with offshore waters. Consistent with these results, nearshore Ω_{ar} values were approximately 40% lower than offshore values, indicating a strong negative correlation between the percentage of pteropod individuals with severe shell dissolution and Ω_{ar} (Fig. 6).

In 2011 and 2013, C_{anth} contributed approximately 22 - 65% of the enriched DIC in the coastal areas over the period of the spring and summer measurements through the top 100 m (Table 1). This contribution lowered average seawater Ω_{ar} values from approximately 1.39 to 1.05 in the nearshore region in 2011, and from 1.46 to 1.08 in 2013. Offshore, the contribution of C_{anth} reduced Ω_{ar} from an average of 2.21 to 1.51 in 2011, and from 2.09 to 1.43 in 2013 since the pre-industrial times. Consequently, based on the newly developed relationships in Figure 6, we estimate that the percentage of pteropods affected with severe dissolution due to the C_{anth} contribution in 2011 increased 19% in the nearshore waters and 26% in the offshore waters (Table 2). In 2013, we estimate C_{anth} had increased the percentage of individuals affected by dissolution by 20% and 25% in nearshore and offshore waters, respectively (Table 2). The 2013 results are comparable to the results for 2011, providing further evidence for increasing incidence of severe dissolution with increasing C_{anth} and decreasing Ω_{ar}. The estimate of pteropod dissolution from C_{anth} is comparable to that reported previously (Bednaršek et al., 2014a), where dissolution was estimated based on the difference between pre-industrial and current DIC values.

The observed relationship between Ω_{ar} and severe shell dissolution suggests that changes

401 in the carbonate chemistry due to C_{anth} are already having an impact on *L. helicina*.
402 Although the percentage of individuals affected by dissolution in the nearshore region is
403 ~22% greater than in the offshore region, the increase due to anthropogenic CO_2 of
404 approximately 20–25% is comparable in both regions. Surprisingly, the relative change
405 in the extent of pteropod dissolution in the offshore regions suggest that they are at least
406 as vulnerable, or perhaps even more vulnerable, to the changes imposed by the C_{anth}
407 uptake over the last several decades. This may be related to the much lower natural
408 variability in offshore waters as compared with the nearshore waters.
409

410 Table 2. Average pre-industrial and current aragonite saturation states (calculated for
411 years 2011 and 2013) and average percentage of individuals affected by severe
412 dissolution in the pre-industrial times and currently for the nearshore and offshore regions
413 of CCLME.
414

Year	Location	Ω_{ar}, preind.	Ω_{ar}, current	% ind. with severe dissolution, preind.	% ind. with severe dissolution, current
2011	nearshore	1.39	1.05	39	58
2013	nearshore	1.46	1.08	36	56
2011	offshore	2.21	1.51	8	34
2013	offshore	2.09	1.43	12	37

415

416 Shell dissolution as observed in pteropods along the west coast of North America affects
417 their swimming abilities (Bednaršek et al, unpublished results), and can potentially
418 enhance predation pressure and increase energetic costs of vital biological processes
419 (Lischka et al., 2011; Wood et al., 2008; Manno et al., 2012). This chronic exposure to
420 undersaturated conditions results in sub-lethal effects of compromised physiological
421 state that may, over longer time periods, affect the overall pteropod population in the
422 CCLME (Weisberg et al., 2016). Given that pteropods are equally abundant nearshore

and offshore (Mackas and Gailbraith, 2012; Bednaršek et al., 2012b), changes due to OA intensification might have ecological implications in both regions. Additionally, the role of pteropods as potentially important prey species requires better understanding of trophic interactions with their predators on the regional level in the CCLME. Integrating pteropods as an independent functional group in end-to-end modeling efforts can help reveal the impacts of potential pteropod biomass decreases on higher trophic levels. Introducing pteropods in such models would require incorporating information on pteropod diet, life-history stages, and physiological and feeding responses, which has recently been reviewed by Bednaršek et al. (2016).

5. Conclusions

By combining chemical and biological studies in the field we are able to provide a clearer picture of the extent of C_{anth} distributions and its likely impact on pteropod shell dissolution. Our results suggest that large-scale declines in the aragonite saturation states of the CCLME resulting from the uptake of C_{anth} in open-ocean and coastal waters are leading to increased incidence of pteropod shell dissolution and potentially creating significant challenges for these organisms. Since the pre-industrial times, pteropod shell dissolution has, on average, increased approximately 20–25% in both nearshore and offshore waters in the CCLME. The capacity of these organisms to acclimatize and adapt to OA, amid concurrent changes in temperature, dissolved oxygen, and other drivers remains largely unknown. Nevertheless, the results shown here clearly indicate that humankind may already be having a significant impact on a species that may play a vital role in this large and important marine ecosystem.

6. Acknowledgments

The National Oceanic and Atmospheric Administration (NOAA) and the National Science Foundation sponsored this work. We specifically thank Libby Jewett and Dwight Gledhill of the NOAA Ocean Acidification Program, Kenneth Mooney and Kathy Tedesco of the NOAA Climate Program, and Dave Garrison of the National Science Foundation for their support. Nina Bednaršek was supported by the NOAA Pacific Marine Environmental Laboratory, the Educational Foundation of America, and the Washington Ocean Acidification Center. This is PMEL contribution number 4355.

7. References

Anderson, L.A., Sarmiento, J.L., 1994. Redfield ratios of remineralization determined by nutrient data analysis. Global Biogeochem. Cycles 8(1), 65–80, doi:10.1029/93GB03318.

Armstrong, J.L., Boldt, J.L., Cross, A.D., Moss, J.H., Davis, N.D., Myers, K.W., Walker, R.V., Beauchamp, D.A., Haldorson, L.J., 2005. Distribution, size, and interannual, seasonal and diel food habits of northern Gulf of Alaska juvenile pink salmon, *Oncorhynchus gorbuscha*. Deep Sea Research Part II 52, 247–265.

Aydin, K.Y., McFarlane, G.A., King, J.R., Megrey, B.A., Myers, K.W., 2005. Linking oceanic food webs to coastal production and growth rates of Pacific salmon (*Oncorhynchus* spp.), using models on three scales. Deep Sea Research Part II 52, 757–780.

468 Barton, A., Hales, B., Waldbusser, G., Langdon, C., Feely, R.A., 2012. The Pacific oyster,
469 *Crassostrea gigas*, shows negative correlation to naturally elevated carbon
470 dioxide levels: Implications for near-term ocean acidification impacts. Limnol.
471 Oceanogr. 57, 698–710, doi:10.4319/lo.2012.57.3.0698.
472 Barton, A., Waldbusser, G.G., Feely, R.A., Weisberg, S.B., Newton, J.A., Hales, B.,
473 Cudd, S., Eudeline, B., Langdon, C.J., Jefferds, I., King, T., Suhrbier, A.,
474 McLaughlin, K., 2015. Impacts of coastal acidification on the Pacific Northwest
475 shellfish industry and adaptation strategies implemented in response.
476 Oceanography 28(2), 146–159, doi:10.5670/oceanog.2015.38.
477 Bates, N.R., Orchowska, M.I., Garley, R., Mathis, J.T., 2013. Summertime calcium
478 carbonate undersaturation in shelf waters of the western Arctic Ocean—how
479 biological processes exacerbate the impact of ocean acidification. Biogeosciences
480 10, 5281–5309, doi:10.5194/bg-10-5281-2013.
481 Bednaršek, N., Tarling, G.A., Bakker, D.C.E., Fielding, S., Jones, E.M., Venables, H.J.,
482 Ward, P., Kuzirian, A., Lézé, B., Feely, R.A., Murphy, E.J., 2012a. Extensive
483 dissolution of live pteropods in the Southern Ocean. Nature Geosci. 5, 881–885,
484 doi:10.1038/ngeo1635.
485 Bednaršek, N., Feely, R.A., Reum, J.C.P., Peterson, W., Menkel, J., Alin, S.R., Hales, B.,
486 2014a. *Limacina helicina* shell dissolution as an indicator of declining habitat
487 suitability due to ocean acidification in the California Current Ecosystem. Proc.
488 Roy. Soc. B 281, 20140123, doi:10.1098/rspb.2014.0123.
489 Bednaršek, N., Tarling, G.A., Bakker, D.C.E., Fielding, S., Feely, R.A., 2014b.
490 Dissolution dominating calcification process in polar pteropods close to the point

of aragonite undersaturation. PLoS ONE 9(10), e109183, doi:10.1371/journal.pone.0109183.

Bednaršek, N., Možina, J., Vogt, M., O'Brien, C., Tarling, G.A., 2012b.The global distribution of pteropods and their contribution to carbonate and carbon biomass in the modern ocean. Earth System Science Data 4(1), 167–186.

Bednaršek, N., Tarling, G.A., Bakker, D.C., Fielding, S., Cohen, A., Kuzirian, A., Montagna, R., 2012c. Description and quantification of pteropod shell dissolution: a sensitive bioindicator of ocean acidification. Global Change Biology 18(7), 2378–2388.

Bednaršek, N., Harvey, C.J., Kaplan, I.C., Feely, R.A. and Možina, J., 2016. Pteropods on the edge: Cumulative effects of ocean acidification, warming, and deoxygenation. *Progress in Oceanography*, *145*, pp.1-24.

Booth, A.T., McPhee, E.E., Chua, P., Kingsley, E., Denny, M., Phillips, R., Bograd, S.J., Zeidberg, L.D., Gilly, W.F., 2012. Natural intrusions of hypoxic, low pH water into nearshore marine environments on the California coast. Cont. Shelf Res. 45, 108–115.

Byrne, R.H., Mecking, S., Feely, R.A., Liu, X., 2010. Direct observations of basin-wide acidification of the North Pacific Ocean. Geophys. Res. Lett. 37, L02601, doi:10.1029/2009GL040999.

Canadell, J.G., Le Quéré, C., Raupach, M.R., Field, C.B., Buitehuis, E.T., Ciais, P., Conway, T.J., Houghton, R.A., Marland, G., 2007. Contributions to accelerating atmospheric CO_2 growth from economic activity, carbon intensity, and efficiency of natural sinks. Proc. Natl. Acad. Sci. USA 104(47), 18866–18870,

514 doi:10.1073/pnas.0702737104.
515 Carpenter, J.H., 1965. The Chesapeake Bay Institute technique for the Winkler dissolved
516 oxygen method. Limnol. Oceanogr. 10(1), 141–143,
517 doi:10.4319/lo.1965.10.1.0141.
518 Carter, B.R., Feely, R.A., Mecking, S., Cross, J. N., Macdonald, A. M., Siedlecki, S. A.,
519 Talley, L. D., Sabine, C. L., Millero, F. J., Swift, J. H., and Dickson, A. G. Two
520 Decades of Pacific Anthropogenic Carbon Storage and Ocean Acidification
521 Along GO-SHIP Sections P16 and P02, Global Biogeochemical Cycles,
522 submitted for publication.
523 Chan, F., Barth, J.A., Lubchenco, J., Kirincich, A., Weeks, H., Peterson, W.T., Menge,
524 B.A., 2008. Emergence of anoxia in the California current large marine
525 ecosystem. Science 319(5865), 920, doi:10.1126/science.1149016.
526 Chan, F., Barth, J.A., Blanchette, C.A., Byrne, R.H., Chavez, F., Cheriton, S.O., Feely,
527 R.A., Friedrich, G., Gaylord, B., Gouhier, T., Hacker, S., Hill, T., Hofmann, G.,
528 McManus, M.A., Menge, B., Nielsen, K.J., Russell, A., Sanford, E., Sevadjian, J.,
529 Washburn, L., Evidence for widespread progression of nearshore ocean
530 acidification in the California Current System, Scientific Reports, submitted for
531 publication.
532 Dickson, A.G., 1990. Thermodynamics of the dissociation of boric acid in synthetic
533 seawater from 273.15 to 298.25 K. Deep-Sea Res., 37; 755-766.
534 Dickson, A.G., Sabine, C.L., Christian, J.R. (Eds.), 2007. Guide to Best Practices for
535 Ocean CO_2 Measurements. PICES Special Publication 3, 191 pp.

536 DOE, 1994. Handbook of Methods for the Analysis of the Various Parameters of the
537 Carbon Dioxide System in Sea Water (Version 2), ORNL/CDIAC-74.
538 Doney, S.C., Balch, W.M., Fabry, V.J., Feely, R.A., 2009a. Ocean acidification: A
539 critical emerging problem for the ocean sciences. Oceanography 22(4), 18–27,
540 doi:10.5670/oceanog.2009.93.
541 Doney, S.C., Fabry, V.J., Feely, R.A., Kleypas, J.A., 2009b. Ocean acidification: The
542 other CO_2 problem. Annu. Rev. Mar. Sci. 1, 169–192.
543 Ekstrom, J.A. Suatoni, L., Cooley, S.R., Pendleton, L.H., Waldbusser, G.G., Cinner, J.E.,
544 Ritter, J., Langdon, C., van Hooidonk, R., Gledhill, D., Wellman, K., Beck, M.W.,
545 Brander, L.M., Rittschof, D., Doherty, C., Edwards, P.E.T., Portela, R., 2015.
546 Vulnerability and adaptation of US shellfisheries to ocean acidification. Nature
547 Clim. Change 5, 207–214, doi:10.1038/NCLIMATE2508.
548 Evans, W., Hales, B., Strutton, P.G., 2013. pCO_2 distributions and air-water CO_2 fluxes in
549 the Columbia River estuary. Estuar. Coast. Shelf Sci. 117, 260–272,
550 doi:10.1016/j.ecss.2012.12.003.
551 Fabry, V.J., Seibel, B.A., Feely, R.A., Orr, J.C., 2008. Impacts of ocean acidification on
552 marine fauna and ecosystem processes. ICES J. Mar. Sci. 65, 414–432.
553 Feely, R.A., Sabine, C.L., Lee, K., Berelson, W., Kleypas, J., Fabry, V.J., Millero, F.J.,
554 2004. Impact of anthropogenic CO_2 on the $CaCO_3$ system in the oceans. Science
555 305(5682), 362–366, doi:10.1126/science.1097329.
556 Feely, R.A., Sabine, C.L., Hernandez-Ayon, J.M., Ianson, D., Hales, B., 2008. Evidence
557 for upwelling of corrosive "acidified" water onto the Continental Shelf. Science
558 320(5882), 1490–1492, doi:10.1126/science.1155676.

559 Feely, R.A., Doney, S.C., Cooley, S.R., 2009. Ocean acidification: Present conditions and
560 future changes in a high-CO_2 world. Oceanography 22(4), 36–47,
561 doi:10.5670/oceanog.2009.95.
562 Feely, R.A., Sabine, C.L., Byrne, R.H., Millero, F.J., Dickson, A.G., Wanninkhof, R.,
563 Murata, A., Miller, L.A., Greeley, D., 2012a. Decadal changes in the aragonite
564 and calcite saturation state of the Pacific Ocean. Global Biogeochem. Cycles 26,
565 GB3001, doi:10.1029/2011GB004157.
566 Feely, R.A., Klinger, T., Newton, J.A., Chadsey, M., 2012b. Scientific Summary of
567 Ocean Acidification in Washington State Marine Waters. NOAA OAR Special
568 Report, 170 pp.
569 Frieder, C.A., Gonzalez, J.P., Bockmon, E.E., Navarro, M.O., Levin, L.A., 2014. Can
570 variable pH and low oxygen moderate ocean acidification outcomes for mussel
571 larvae? Global Change Biol. 20, 754–764.
572 Gattuso, J.-P., Hansson, L., 2011. Ocean acidification: Background and history. In:
573 Gattuso, J.-P., Hansson, L. (Eds.), Ocean Acidification. Oxford Univ. Press,
574 Oxford, pp. 1–20.
575 Gattuso, J.-P., Magnan, A., Bille, R., Cheung, W.W.L., Howes, E.L., Joos, F., Allemand,
576 D., Bopp, L., Cooley, S.R., Eakin, C.M., Hoegh-Guldberg, O., Kelly, R.P.,
577 Pörtner, H.-O., Rogers, A.D., Baxter, J.M., Laffoley, D., Osborn, D., Rankovic,
578 A., Rochette, J., Sumaila, U.R., Treyer, S., Turley, C., 2015. Contrasting futures
579 for ocean and society from different anthropogenic CO_2 emission scenarios.
580 Science 349(6243), aac4722, doi:10.1126/science.aac4722.
581 Gaylord, B., Hill, T.M., Sanford, E., Lenz, E.A., Jacobs, L.A., Sato, K.N., Russell, A.D.,

582 Hettinger, A., 2011. Functional impacts of ocean acidification in an ecologically
583 critical foundation species. J. Exp. Biol. 214, 2586–2594.
584 Gaylord, B., Kroeker, K.J., Sunday, J.M., Anderson, K.M., Barry, J.P., Brown, N.E.,
585 Connell, S.D., Dupont, S., Fabricius, K.E., Hall-Spencer, J.M., Klinger, T.,
586 Milazzo, M., Munday, P.L., Russell, B.D., Sanford, E., Schreiber, S.J.,
587 Thiyagarajan, V., Vaughan, M.L.H., Widdicombe, S., Harley, C.D.G., 2015.
588 Ocean acidification through the lens of ecological theory. Ecology 96, 3–15.
589 Grantham, B.A., Chan, F., Nielsen, K.J., Fox, D.S., Barth, J.A., Lubchenco, J., Menge,
590 B.A., 2004. Upwelling-driven nearshore hypoxia signals ecosystem and
591 oceanographic changes in the northeast Pacific. Nature 429(6993), 749–754,
592 doi:10.1038/nature02605.
593 Groot, C., Margolis, L. (Eds.), 1991. Pacific Salmon Life Histories. UBC Press,
594 Vancouver, Canada.
595 Gruber, N., Hauri, C., Lachkar, Z., Loher, D., Frölicher, T.L., Plattner, G.-K., 2012.
596 Rapid progression of ocean acidification in the California Current System.
597 Science 337 (6091), 220–223.
598 Guinotte, J.M., Fabry, V.J., 2008. Ocean acidification and its potential effects on marine
599 ecosystems. Ann. NY Acad. Sci. 1134, 320–342, doi:10.1196/annals.1439.013.
600 Hales, B., Karp-Boss, L., Perlin, A., Wheeler, P., 2006. Oxygen production and carbon
601 sequestration in an upwelling coastal margin. Global Biogeochem. Cycles 20,
602 GB3001, doi:10.1029/2005GB002517.

603 Harris, K.E., DeGrandpre, M.D., Hales, B., 2013. Aragonite saturation state dynamics in
604 a coastal upwelling zone. Geophys. Res. Lett. 40, 2720–2725,
605 doi:10.1002/grl.50460.
606 Hauri, C., Gruber, N., Vogt, M., Doney, S.C., Feely, R.A., Lachkar, Z., Leinweber, A.,
607 McDonnell, A.M.P., Munnich, M., Plattner, G.-K., 2013. Spatiotemporal
608 variability and long-term trends of ocean acidification in the California Current
609 System. Biogeosciences 10, 193–216, doi:10.5194/bg-10-193-2013.IPCC, 2013.
610 Climate Change 2013: The Physical Science Basis. Contribution of Working
611 Group I to the Fifth Assessment Report of the Intergovernmental Panel on
612 Climate Change. Stocker, T.F., Qin, D., Plattner, G.-K., Tignor, M., Allen, S.K.,
613 Boschung, J., Nauels, A., Xia, Y., Bex, V., Midgley, P.M. (Eds.). Cambridge
614 University Press, Cambridge, UK and New York, NY, 1535 pp. Johnson, K.M.,
615 King, A.E., Sieburth, J.M., 1985. Coulometric TCO_2 analyses for marine studies;
616 an introduction. Mar. Chem. 16, 61–82.
617 Hettinger, A., Sanford, E., Hill, T.M., Russell, A.D., Sato, K.N., Hoey, J., Forsch, M.,
618 Page, H.N., Gaylord, B., 2012. Persistent carry-over effects of planktonic
619 exposure to ocean acidification in the Olympia oyster. Ecology 93, 2758–2768.
620 Hickey, B. M., 1979. The California Current system – Hypotheses and facts, Prog.
621 Oceanogr. 8, 191-279, doi: 10.1016/0079-6611(79)90002-8.
622 Hofmann, G.E., Todgham, A.E., 2010. Living in the now: Physiological mechanisms to
623 tolerate a rapidly changing environment. Annu. Rev. Mar. Physiol. 72, 127–145.

624 Johnson, K.M., Sieburth, J.M., Williams, P.J.L., Brändström, L., 1987. Coulometric total
625 carbon dioxide analysis for marine studies: automation and calibration. Mar.
626 Chem. 21, 117–133.
627 IPCC, 2013: Climate Change 2013: The Physical Science Basis. Contributions of
628 Working Group I to the Fifth Assessment Report of the Intergovernmental Panel
629 on Climate Change, Stocker, T.F., D. Qin, G. –K. Plattner, M. Tignor, S.K. Allen,
630 J. Boschung, A. Nauels, Y. Xia, V. Bex and P.M. Midgley, (eds). Cambridge
631 University Press, Cambridge, United Kingdom and NY, USA 1535 pp.
632 Kroeker, K.J., Kordas, R.L., Crim, R., Hendriks, I.E., Ramajo, L., Singh, G.S., Duarte,
633 C.M., Gattuso. J.-P., 2013. Impacts of ocean acidification on marine organisms:
634 Quantifying sensitivities and interaction with warming. Glob. Change Biol. 19,
635 1884–1896, doi:10.1111/gcb.12179.
636 Lee, K., T.-W. Kim, R.H. Byrne, F.J. Millero, R.A. Feely, and Y.-M. Liu (2010): The
637 universal ratio of boron to chlorinity for the North Pacific and North Atlantic
638 oceans. Geochim. Cosmochim. Acta, 74(6), 1801–1811, doi:
639 10.1016/j.gca.2009.12.027.
640 Lewis, E., Wallace, D.W.R. 1998. Program developed for CO_2 System Calculations.
641 ORNL/CDIAC-105, Carbon Dioxide Information Analysis Center, Oak Ridge
642 National Laboratory, Oak Ridge, Tenn. Available online at
643 http://cdiac.ornl.gov/ftp/co2sys/CO2SYS_calc_DOS_v1.05/cdiac105.pdf.
644 Lischka S, Buedenbender J, Boxhammer T, Riebesell U., 2011. Impact of ocean
645 acidification and elevated temperatures on early juveniles of the polar shelled
646 pteropod *Limacina helicina*: mortality, shell degradation, and shell growth.

Biogeosciences 8, 919– 932.

Liu, X., Patsavas, M.C., Byrne, R.H., 2011. Purification and characterization of meta-cresol purple for spectrophotometric seawater pH measurements. Environ. Sci. Technol. 45(11), 4862–4868.

Lueker, T.J., Dickson, A.G., Keeling, C.D., 2000. Ocean pCO_2 calculated from dissolved inorganic carbon, alkalinity, and equations for K1 and K2: Validation based on laboratory measurements of CO_2 in gas and seawater at equilibrium. Mar. Chem. 70(1–3), 105–119.

Mackas, D.L., Galbraith, M.D., 2012. Pteropod time-series from the NE Pacific. ICES J. Mar. Sci. 69(3), 448–459. doi:10.1093/icesjms/fsr163.

Manno C, Morata N, Primicerio R., 2012. Limacina retroversa's response to combined effects of ocean acidification and sea water freshening. Estuar. Coast. Shelf Sci. 113, 163 – 171.

Mathis, J.T., Cross, J.N., Monacci, N., Feely, R.A., Stabeno, P.J., 2014a. Evidence of prolonged aragonite undersaturations in the bottom waters of the southern Bering Sea shelf from autonomous sensors. Deep-Sea Res. II 109, 125–133, doi:10.1016/j.dsr2.2013.07.019.

Mathis, J.T., Grebmeier, J.G., Hansell, D.A., Hopcroft, R.R., Kirchman, D.L., Lee, S.H., Moran, S.B., Bates, N.R., VanLaningham, S., Cross, J.N., Cai, W.J., 2014b. Carbon biogeochemistry of the western Arctic: Primary production, carbon export and the controls on ocean acidification. In: Grebmeier, J.M., Maslowski, W. (Eds.), The Pacific Arctic Region: Ecosystem Status and Trends in a Rapidly

669 Changing Environment. Springer Science+Business Media, Dordrecht, pp. 223–
670 268.
671 Mathis, J.T., Cross, J.N., Evans, W., Doney, S.C., 2015. Ocean acidification in the
672 surface waters of the Pacific-Arctic boundary regions. Oceanography 28(2), 122–
673 135, doi:10.5670/oceanog.2015.36.
674 Millero, F.J., 1995. Thermodynamics of the carbon-dioxide system in the oceans.
675 Geochim. Cosmochim. Acta 59, 661–677.
676 Millero, F.J., Zhang, J.Z., Lee, K., Campbell, D.M., 1993. Titration alkalinity of
677 seawater. Mar. Chem. 44, 153–165.
678 Mucci, A., 1983. The solubility of calcite and aragonite in seawater at various salinities,
679 temperatures, and one atmosphere total pressure. Am. J. Sci. 283, 780–799.
680 Ono, T., Watanabe, S., Okuda, K., Fukasawa, M., 1998. Distribution of total carbonate
681 and related properties in the North Pacific along 30°N. J. Geophys. Res.-Oceans
682 103, 30873–30883.
683 Orr, J.C., Fabry, V.J., Aumont, O., Bopp, L., Doney, S.C., Feely, R.A., Gnanadesikan,
684 A., Gruber, N., Ishida, A., Joos, F., Key, R.M., Lindsay, K., Maier-Reimer, E.,
685 Matear, R., Monfray, P., Mouchet, A., Najjar, R.G., Plattner, G.K., Rodgers, K.B.,
686 Sabine, C.L., Sarmiento, J.L., Schlitzer, R., Slater, R.D., Totterdell, I.J., Weirig,
687 M.F., Yamanaka, Y., Yool, A., 2005. Anthropogenic ocean acidification over the
688 twenty-first century and its impact on calcifying organisms. Nature 437, 681–686.
689 Rykaczewski, R.R., Dunne, J.P., 2010. Enhanced nutrient supply to the California
690 Current Ecosystem with global warming and increased stratification in an earth
691 system model. Geophys. Res. Lett. 37(21), L21606, doi:10.1029/2010GL045019.

692 Sabine, C.L., Feely, R.A., Millero, F.J., Dickson, A.G., Langdon, C., Mecking, S.,
693 Greeley, D., 2008. Decadal changes in Pacific carbon. J. Geophys. Res. 113,
694 C07021, doi:10.1029/2007JC004577.
695 Sabine, C.L., Tanhua, T., 2010. Estimation of anthropogenic CO_2 inventories in the ocean.
696 Annu. Rev. Mar. Sci. 2, 175–198, doi:10.1146/annurev-marine-120308-080947.
697 Siedlecki, S.A., I. Kaplan, A.J. herman, T.T. Nguyen, N.A. Bond, J.A. Newton, G.D.
698 Williams, W.T. Peterson, S.R. Alin, and R.A. Feely, 2016. Experiments with
699 seasonal forecasts of ocean conditions for the northern region of the of the
700 California Current upwelling system, Scientific Reports, 6: 27203:
701 doi:10.1038.srep/27203
702 Somero, G.N., Beers, J., Chan, F., Hill, T., Klinger, T., Litvin, S., 2016. What changes in
703 the carbonate system, oxygen, and temperature portend for the northeastern
704 Pacific Ocean: A physiological perspective. Bioscience 66, 14–26,
705 doi:10.1093/biosci/biv162.
706 Thomson, R.E., Hickey, B.M., LeBond, P.H., 1989. The Vancouver Island Coastal
707 Current: Fisheries barrier and conduit, in Effets of Ocean Variability on
708 Recruitment and an Evaluation of parameters Used in Stock Assessment Models,
709 vol. 108, edited by R. J. Beamish and G. McFarlane, pp. 265-296, Dept. of Fish.
710 and Oceans, Ottawa, Ont., Canada.
711 Thomson, R.E., Krassovski, M.V., 2010. Poleward reach of the California Undercurrent
712 Extension, J. Geophys. Res., 115, C09027, doi:10.1029/2010JC006280.

713 Turi, G., Lachkar, Z., Gruber, N., Munnich, M., 2016. Climatic modulation of recent
714 trends in ocean acidification in the California Current System, Environ. Res. Lett.
715 11 (2016) 014007 doi:10.1088/1748-9326/11/1/014007.

716 UNESCO, 1994. Protocols for the Joint Global Ocean Flux Study (JGOFS) Core
717 Measurements. United Nations Educational, Scientific, and Cultural Organization,
718 http://ijgofs.whoi.edu/Publications/Report_Series/JGOFS_19.pdf.Waldbusser,
719 G.G., Hales, B., Langdon, C.J., Haley, B.A., Schrader, P., Brunner, E.L., Gray,
720 M.W., Miller, C.A., Gimenez, I., 2015. Saturation-state sensitivity of marine
721 bivalve larvae to ocean 709 acidification. Nature Clim. Change 5, 273–280,
722 doi:10.1038/NCLIMATE2479.

723 Waldbusser, G.G., B. Hales, C.J. Langdon, B.A. Haley, P. Schrader, E.L Brunner, M.W.
724 Gray, C.A. Miller and I. Gimenez (2015): Saturation state sensitivity of marine
725 bivalve larvae to ocean acidification, Nat. Clim. Change **5:** 273-280.
726 doi:10.1038/nclimate2479

727 Weisberg, S.B., N. Bednaršek, R.A. Feely, F. Chan, A.B. Boehm, M. Sutula, J.L.
728 Ruesink, B. Hales, J.L. Largier, and J.A. Newton (2016): Water quality criteria
729 for an acidifying ocean: Challenges and opportunities. Ocean Coastal Manage.,
730 126, 31–41, doi: 10.1016/j.ocecoaman.2016.03.010.

731 Wood H.L., Spicer J.I., Widdicombe S., 2008. Ocean acidification may increase
732 calcification rates, but at a cost. Proc. R. Soc. B 275, 1767– 1773.

733 Wootton, J.T., Pfister, C.A., Forester, J.D., 2008. Dynamic patterns and ecological
734 impacts of declining ocean pH in a high-resolution multi-year dataset. Proc. Natl.
735 Acad. Sci. USA 105, 18848–18853.

Figure and table captions

Figure 1. Map of the station locations for the 2007 West Coast cruise. The black line shows the cruise track. The 2011, 2012, and 2013 cruises included subsets of these stations and, in some cases, a few additional stations.

Figure 2. Maps of surface ocean pH_T values for the 2007, 2011, 2012, and 2013 cruises. The 2011 map includes the shore-based intertidal data.

Figure 3. Maps of surface DIC concentrations in µmol kg^{-1} for the 2007, 2011, 2012, and 2013 cruises. The nearshore upwelling regions are delineated by DIC concentrations in excess of 2050 µmol kg^{-1}. Black dots indicate measurement locations. Open circles on the 2011 and 2013 cruises indicate stations where both chemical and biological samples were taken.

Figure 4. Aragonite saturation state at the surface, 25 m, 55 m, and 105 m during the 2013 West Coast survey.

Figure 5. Vertical sections of: (A) dissolved oxygen, (B) pCO_2, (C) pH_T, and (D) Ω_{ar} along the 2013 Line 6 stations off Newport, OR. Black dots indicate measurement locations and the isolines lines in (A) and (B) show the potential density in kg m^{-3}.

Figure 6. Percentage of individuals affected by severe dissolution as a function of aragonite saturation state (integrated over the upper100 m) for the 2011 (open circles) and 2013 (closed circles) data. The dashed lines show the 95% confidence interval for the logarithmic function.

Figure 7. Distribution of C_{anth} in µmol kg^{-1} at the surface, 25 m, 55 m, and 105 m depth for the 2013 West Coast survey.

Figure 8. Plot of C_{bio} vs C_{anth} in offshore and nearshore waters in the California Current

Large Marine Ecosystem. The simple schematic in the upper right is a zonal section of the coast with offshore being to the left, and with the mean path of upwelling water indicated as a red arrow. Error bars express standard deviations for various estimates from each region and depth (Table 1) rather than uncertainty, which is 1σ of ±10 μmol kg^{-1} for C_{bio} and C_{anth}.

Table 1. Anthropogenic carbon (C_{anth}), remineralized carbon (C_{bio}) and anthropogenic percentage of total enriched carbon ($\%C_{anth}$) by region (W: Washington, O: Oregon, NC: Northern California, SC: Southern California), cruise year, and depth for averages of gridded coastal properties shoreward of the 200 m isobath (left columns) and for the northwestern stations occupied offshore of each region (right columns). All values are expressed in μmol kg^{-1}. Estimated average uncertainty is approximately ±10 μmol kg^{-1} (1σ). Column averages are calculated weighting all regions and years equally. Negative C_{bio} values suggest either net autotrophy or physically derived oxygen supersaturation.

Table 2. Average pre-industrial and current aragonite saturation states (calculated for years 2011 and 2013) and average percentage of individuals affected by severe dissolution in the pre-industrial times and currently for the nearshore and offshore regions of CCLME.

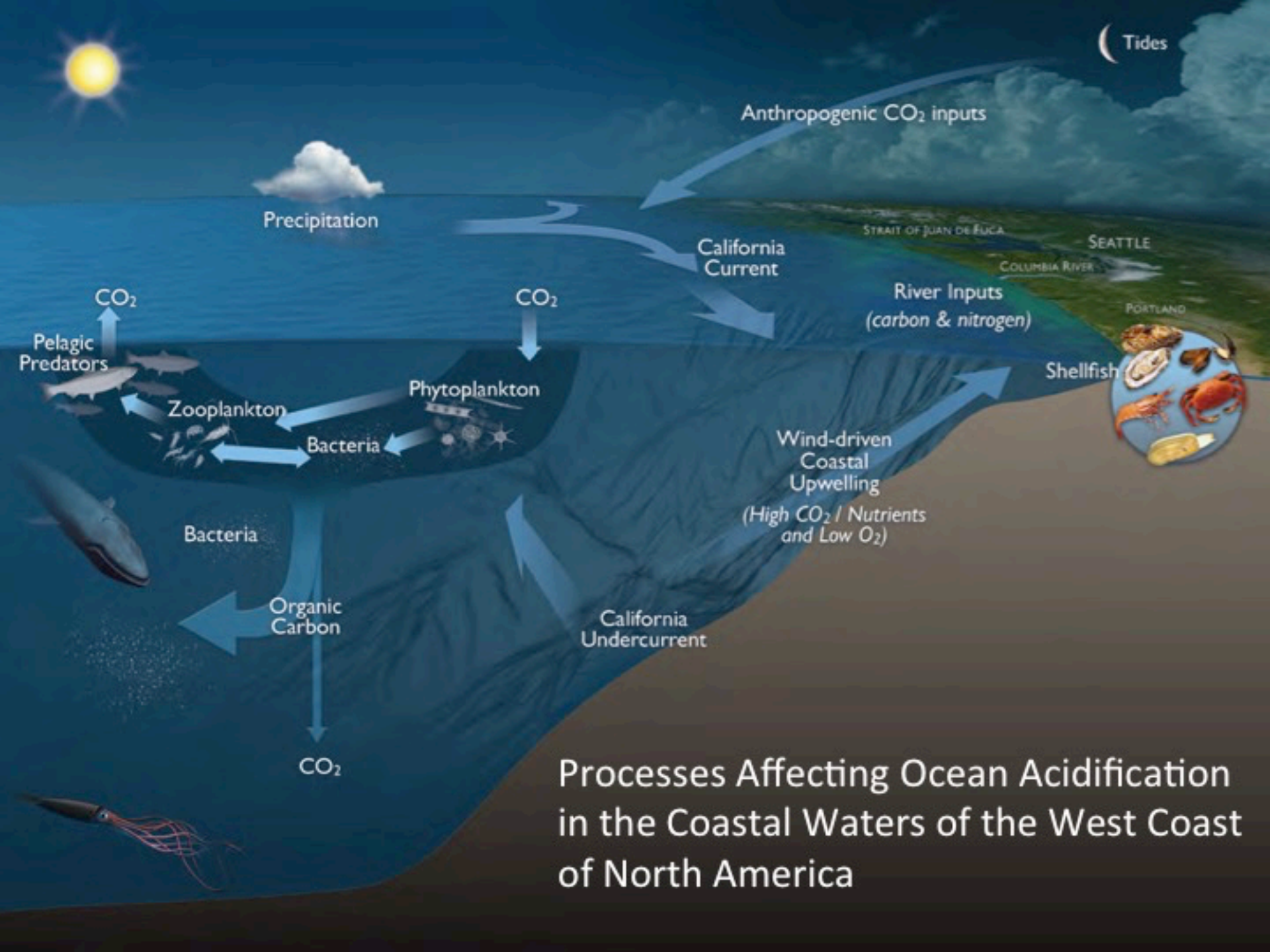
Tides
Anthropogenic CO_2 inputs
Precipitation
California Current
Strait of Juan de Fuca
Seattle
Columbia River
Portland
River Inputs
(carbon & nitrogen)
CO_2
CO_2
Pelagic Predators
Phytoplankton
Zooplankton
Bacteria
Shellfish
Wind-driven Coastal Upwelling
(High CO_2 / Nutrients and Low O_2)
Bacteria
Organic Carbon
California Undercurrent
CO_2
Processes Affecting Ocean Acidification in the Coastal Waters of the West Coast of North America